Sliding Mode Control of Tethered Drone: Take-off and Landing under Turbulent Wind conditions

Zakeye Azaki, Jonathan Dumon, Nacim Meslem, Ahmad Hably

Sliding Mode Control of Tethered Drone: Take-off and Landing under Turbulent Wind conditions

Zakeye AZAKI, Jonathan DUMON, Nacim MESLEM, Ahmad HABLY

***Abstract*— Tethered flight is a highly nonlinear and uncertain process that requires robust control approaches to master its operation. However, there have been only a few researches on the control of the take-off and landing phases of these systems. This paper proposes a sliding mode controller, for tethered drones, to track a desired flight trajectory. Additionally, a three-dimensional Extended Kalman filter is integrated into the control strategy to estimate and compensate for aerodynamic disturbances. Controller performance is evaluated against wind turbulence conditions and modeling uncertainties. The results are compared with those of a non-linear feedback linearization controller.**

Keywords: Tethered drones, Sliding Mode Control, Aerodynamic Disturbances, Extended Kalman Filter.

I. Introduction

Tethered drones have a wide range of potential applications. In this present work we focus on using them in the specific field of airborne wind energy (AWE). The purpose of AWE systems is to harvest high-altitude wind energy and convert it into electrical energy [1], [2]. There are two classes of AWE systems, depending on where energy is produced [3]. On the one hand, there are on-board production systems where classical wind turbines are mounted on flying wings and transmit electricity to the ground via conductive tethers. On the other hand, there are on-ground production systems whereby the device follows a predetermined trajectory and produces aerodynamic lift and drag forces transmitted via a tether to an on-ground station for conversion into electricity. Different types of wings are used: soft, rigid, etc.

The dynamics of the AWE systems are strongly nonlinear and parameter-dependant. Uncertainties and external disturbances have to be handled by the appropriate controllers. Moreover, several partially known or unknown forces affect the AWE system. These forces include aerodynamic forces that are affected by wind speed and direction, which can be difficult to measure. As a result, the AWE system becomes very uncertain and its control performance is significantly impacted due to this fact.

As a critical challenge for AWE Systems, automating tethered flight must be mastered to achieve operating success. It is essential to recognize that we are dealing with a broad spectrum of automatic control strategies that must perform robustly under extreme operating conditions. The system needs to operate in different phases, including take-off and landing, as well as power generation. Most of the literature addresses the problem of control during power generation

The authors are with GIPSA-lab, Univ. Grenoble Alpes, CNRS, Grenoble-INP. (zakeye.azaki, jonathan.dumon, nacim.meslem, ahmad.hably)@gipsa-lab.grenoble-inp.fr

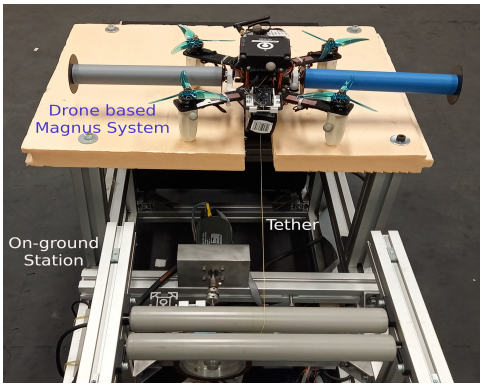

Fig. 1: Drone-based Magnus AWE prototype.

[4], [5].

Few studies have been conducted to assign the phases of take-off and landing of AWE systems. One solution is to use a multicopter as described in [6] for the take-off and landing phases. In that study, the motion of the AWE system is considered in 2D. Hierarchical feedback controller-based 3D control strategy for an untethered system was presented in [7]. However, the proposed control strategy showed a decline in performance when exposed to turbulent wind.

In this present work, we have focused on the problem of control during the vertical take-off and landing of a drone-based Magnus system for an on-ground production application. In our previous work [8], the control strategy based on the 3D feedback linearization technique (FL-PID) has been designed to deal with a part of the system's non-linearities. On other hand, integral actions have been added in the closed loop to cope with the neglected (considered as disturbances) unknown forces. Although the results in [8] showed that the (FL-PID) control strategy provides good tracking performance for low and homogeneous wind speeds, however for turbulent and extreme wind speed conditions, the neglected aerodynamic forces, that was considered as disturbances, become significant and affect the desired behavior of the system.

In light of this, the present paper proposes to tackle the control problem through a 3D robust Nonlinear Sliding Mode Control (SMC). For this, we based on the first order SMC [9]. In addition, it is of great interest to estimate the unknown forces acting on the system in order to obtain a more precise model of the system and further master its dynamical behavior. To do this, we have implemented an Extended Kalman filter (EKF) to estimate online these unknown forces. These estimates are then integrated as feed-forward into the control design to

anticipate the effects of disturbances and other external inputs on the system's output, thus improving the performance of the SMC to counteract these disturbances. The overall SMC-augmented with feed-forward control is referred as (FF-SMC). To validate the performance and robustness of this control strategy, (FF-SMC) is compared to the (FL-PID) control. The paper ends with some conclusions and future work.

Paper Organization: In section II we illustrate the system's 3D mathematical model. We describe the design of the (FF-SMC) control strategy in Section III. Section IV represents the realistic simulator and the wind speed model utilized to generate simulations. Lastly, in section V we present some results that validate the robustness of the control strategy.

II. Control Inputs and Mathematical Model

In this section, we recapitulate the mathematical model of the system. The detailed derivation of this model can be found in our previous work [8] for interested readers. This simplified model has been specifically derived to design a control strategy for the take-off and landing phases of the AWE system. However, more complex model is used for simulation testing as is described in section IV.

The system under study is the drone-based AWE system and it is represented in Fig. 1. This system is composed of two main elements: the first one is a flying device composed of Magnus wing fixed to a drone with a combined mass denoted by m_K. The second one is an on-ground winch of inertia I_W, radius R_W, and mass $m_W = \frac{I_W}{R_W^2}$. Both elements are connected through a tether. Note that the tether model has not been considered in the dynamical model. On the contrary, it is assumed that the tether of length r is taut and approximated as a straight line. This assumption could still be of less importance for small tether length where drag and linear mass is negligible w.r.t tether tension. The tether traction force T_T is derived from the rotational equilibrium on the base of the on-ground winch as follows,

$$T_T = u_r + m_W \ddot{r} + F_f \tag{1}$$

where u_r is the on-ground winch motor torque and F_f represents the dry friction of the on-ground winch.

The system is considered as a rigid point mass represented by its polar position vector $\boldsymbol{\xi} = [r, \eta, \beta]^T$ where r is the tether length, η is the azimuth angle and β is the elevation angle. The translation velocity of the flying device $\mathbf{v}_k$ can be decomposed, in the spherical coordinate system, into a radial velocity component $v_{k,r} = \dot{r}$, an azimuthal velocity component $v_{k,\eta} = r\dot{\eta}c\beta$ and a polar velocity component $v_{k,\beta} = r\dot{\beta}$. The acceleration components are derived from differentiation of $\mathbf{v}_k$ with respect to time as follows

$$\dot{\mathbf{v}}_k = \begin{bmatrix} \ddot{r} \\ r\ddot{\eta}c_\beta \\ r\ddot{\beta} \end{bmatrix} + \begin{bmatrix} -r\dot{\beta}^2 - r\dot{\eta}^2 c_\beta^2 \\ 2\dot{r}\dot{\eta}c_\beta - 2r\dot{\eta}\dot{\beta}s_\beta \\ 2\dot{r}\dot{\beta} + r\dot{\eta}^2 c_\beta s_\beta \end{bmatrix} \tag{2}$$

where 's' and 'c' refer respectively to sine and cosine functions. Based on the fundamental principle of dynamics, a 3D nonlinear model of the system can be derived:

$$\ddot{\boldsymbol{\xi}} = \underbrace{\begin{bmatrix} \frac{1}{m_K+m_W}[m_K(r\dot{\beta}^2 + r\dot{\eta}^2 c_\beta^2) - Ps_\beta + u_T] \\ \frac{1}{rc_\beta}[-2\dot{r}\dot{\eta}c_\beta + 2r\dot{\eta}\dot{\beta}s_\beta] \\ -\frac{1}{r}[2\dot{r}\dot{\beta} + r\dot{\eta}^2 c_\beta s_\beta + \frac{1}{m_K}Pc_\beta] \end{bmatrix}}_{\mathbf{B}(\boldsymbol{\xi},\dot{\boldsymbol{\xi}})} + \underbrace{\begin{bmatrix} -\frac{1}{m_K+m_W} & 0 & 0 \\ 0 & \frac{1}{m_K r c_\beta} & 0 \\ 0 & 0 & \frac{1}{m_K r} \end{bmatrix}}_{\mathbf{A}(\boldsymbol{\xi},\dot{\boldsymbol{\xi}})} \left(\underbrace{\begin{bmatrix} u_r \\ u_\eta \\ u_\beta \end{bmatrix}}_{\mathbf{u}} + \underbrace{\begin{bmatrix} -F_{u,r} \\ F_{u,\eta} \\ F_{u,\beta} \end{bmatrix}}_{\mathbf{F}_u} \right) \tag{3}$$

where P is the system's weight. The unknown forces vector $\mathbf{F}_u$ could be viewed as composition in between the Magnus aerodynamic forces $\mathbf{F}_a$, the on-ground dry friction $\mathbf{F}_f$ and the forces due to propeller performance variation and due for example to the embedded battery voltage variation $\mathbf{F}_p$,

$$\begin{cases} F_{u,r} = F_{a,r} + F_{p,r} + F_f \\ F_{u,\eta} = F_{a,\eta} + F_{p,\eta} \\ F_{u,\beta} = F_{a,\beta} + F_{p,\beta} \end{cases} \tag{4}$$

We assume that the control inputs of the system consist of the on-ground winch motor torque u_r and the drone's Euler angles $\boldsymbol{\Theta} = [\phi, \theta, \psi]^T$ and thrust force $\mathbf{T}_D$. The thrust force $\mathbf{T}_D$ is represented by its projections u_T, u_η and u_β into the radial, azimuthal and polar directions respectively. For this, the control variables could be described as u_T and the control input vector $\mathbf{u} = [u_r, u_\eta, u_\beta]^T$. The computation of the desired values of this control variables is illustrated in the section III.

One can notice that the proposed model (3) is invalid for a tether length $r = 0$ and/or $\beta = \frac{\pi}{2}$ since the system is in a singular configuration. As such a configuration is undesirable in practice and may lead to unbounded response, we define an acceptable flying region $\boldsymbol{\Omega}$ which is bounded by the following constraints,

- the flying device is docked to a support at $r \neq 0$,
- the tether's elevation is such that $\beta \leq \beta_{max}$ where $\beta_{max} < \frac{\pi}{2}$,
- maximum allowable wind speed of 10m/s have been established.

The acceptable flying region $\boldsymbol{\Omega}$ is crucial for ensuring the safe and stable operation of the system, and its boundaries was carefully defined and considered in simulations.

In Table I, we represent the involved parameters of model (3) corresponding to the prototype shown in Fig. 1.

TABLE I: Physical Parameters of our prototype

Parameter	Definition	Value
m_K	Mass of the flying device	1.4 kg
m_W	Mass of the on-ground station rotor	0.0481 kg
R_M	radius of the Magnus cylinder	0.04 m
l_M	length of the Magnus cylinder	0.6 m
ρ	Air density	1.293 kg/m^3

III. Position Control

A. Feedback Formulation

Feedback Linearization is applied to obtain the desired control input $\mathbf{u}_d = [u_{d,r}, u_{d,\eta}, u_{d,\beta}]^T$ as:

$$\mathbf{u}_d = \mathbf{A}^{-1}(\boldsymbol{\xi}, \dot{\boldsymbol{\xi}}) * [\mathbf{u}_\xi - \mathbf{B}(\boldsymbol{\xi}, \dot{\boldsymbol{\xi}})] \tag{5}$$

with $*$ corresponds to matrix multiplication. $\mathbf{u}_\xi = [u_{\xi,r}, u_{\xi,\eta}, u_{\xi,\beta}]^T$ is the virtual input vector. To design this virtual input $\mathbf{u}_\xi$, we have based on SMC.

It is known that, SMC policy entails two phases: sliding surface design and then control input design. In the first phase, the sliding surface is chosen with an additional integral term for each loop $q \in \{r, \eta, \beta\}$ as:

$$S_q = \dot{e_q} + \alpha_{1,q} e_q + \alpha_{0,q} \int_0^t e_q d\tau \tag{6}$$

where $e_q = q - q_d$ is the tracking error for each $q \in \{r, \eta, \beta\}$. The coefficients $\alpha_{0,q} > 0$ and $\alpha_{1,q} > 0$ are strictly positive tuning parameters. Through these parameters, the system characteristics may be considered while defining the sliding surface. Consequently, the specifications are met as the system achieves the sliding surface.

Now that the sliding surface has been defined, the next phase is to design a control law steering the system trajectories to the sliding surface in finite time despite the presence of model imprecision and of disturbances (4). To accomplish this, we use the first order SMC for each loop $q \in \{r, \eta, \beta\}$ as:

$$u_{\xi,q} = \ddot{q}_d - \alpha_{1,q}\dot{e_q} - \alpha_{0,q} e_q - \boldsymbol{k}_q \mathbf{sgn}(\boldsymbol{S}_q) \tag{7}$$

B. Feed-forward Formulation

As stated in the previous section, the AWE system is susceptible to a variety of unmeasured forces as illustrated in (4), which have an impact on the precision and robustness of the system's tracking of a given trajectory. Hence, integrating these forces into the control design is crucial for stable and high performing flight. Then, the control law (5) is enhanced as follows:

$$\mathbf{u}_d = \mathbf{A}^{-1}(\boldsymbol{\xi}, \dot{\boldsymbol{\xi}}) * [\mathbf{u}_\xi - \mathbf{B}(\boldsymbol{\xi}, \dot{\boldsymbol{\xi}}) - \mathbf{A}(\boldsymbol{\xi}, \dot{\boldsymbol{\xi}}) * \mathbf{F}_u] \tag{8}$$

This control law can be formalized as combined feed-forward plus feedback control:

$$\mathbf{u}_d = \underbrace{\mathbf{A}^{-1}(\boldsymbol{\xi}, \dot{\boldsymbol{\xi}}) * [\mathbf{u}_\xi - \mathbf{B}(\boldsymbol{\xi}, \dot{\boldsymbol{\xi}})]}_{\mathbf{u}_b} \underbrace{-\mathbf{F}_u}_{\mathbf{u}_f} \tag{9}$$

Such that $\mathbf{u}_b$ is the feedback term of the proposed strategy while $\mathbf{u}_f$ is the feed-forward term.

C. Disturbance Estimation

In order to implement the proposed control law (9), it is essential to have accurate measurements of the disturbance forces $\mathbf{F}_u$. However, obtaining these measurements may prove to be a challenge. For example the aerodynamic forces $\mathbf{F}_a$ acting on the system are difficult to measure directly and they are affected by time-dependent variables such as wind speed and direction. This presents a significant obstacle for the implementation of the control law, as the system's performance relies on the ability to accurately measure and compensate for these disturbances. Furthermore, this difficulty in measuring aerodynamic forces is not unique, as other sources of disturbance such as the ones caused by propellers performance variation $\mathbf{F}_p$ can also be hard to measure accurately.

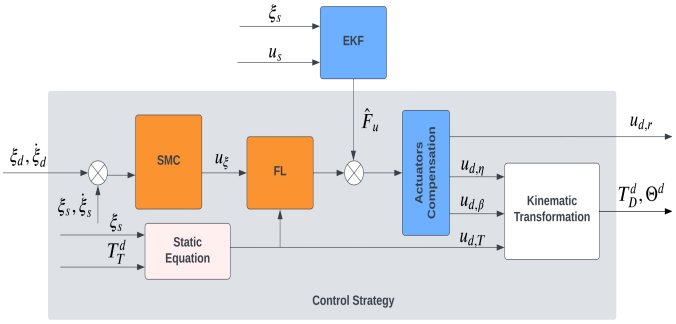

Fig. 2: Block diagram illustrating the (FF-SMC) strategy.

Thus, it is of great interest to estimate the unknown forces $\mathbf{F}_u$. A discrete Extended Kalman filter (EKF) is synthesized to compute online the estimated unknown force vector $\hat{\mathbf{F}}_u$ using the system's output data at hand presented by the measured or simulated states $\mathbf{y} = \boldsymbol{\xi}_s$ and simulated control inputs $\mathbf{u}_s$. The EKF implemented in this work is the extended version, into the 3D frame, of the EKF developed and studied in our work [10]. An augmented model of (3), is necessary to accomplish this task. It is important to note that in this augmented model, the unknown forces outlined in (4) should be treated as state variables with zero dynamics. This augmented model is read:

$$\begin{bmatrix} \ddot{\boldsymbol{\xi}} \\ \dot{\mathbf{F}}_u \end{bmatrix} = \begin{bmatrix} \mathbf{B}(\boldsymbol{\xi}, \dot{\boldsymbol{\xi}}) + \mathbf{A}(\boldsymbol{\xi}, \dot{\boldsymbol{\xi}}) * [\mathbf{u} + \mathbf{F}_u] \\ \mathbf{0} \end{bmatrix} \tag{10}$$

A well-known fact is that the performance of an EKF is primarily dependent upon the tuning of its weighting matrices,i.e., the measurement noise covariance matrix $\mathbf{R}$ and the process noise covariance matrix $\mathbf{Q}$. In our research, we have chosen to increase the eigenvalues in $\mathbf{Q}$ matrix corresponding to the unknown additive forces. By doing so, we aim to ensure that the filter gives more weight to the disturbance dynamics, which are more uncertain, in comparison to the other dynamics of the system. However, the measurements are accurate and reliable, and thus the $\mathbf{R}$ matrix should have small eigenvalues compared to $\mathbf{Q}$. Therefore, based on the estimation values, the (FF-SMC) control strategy, presented in Fig. 2, is developed as:

$$\mathbf{u}_d = \mathbf{A}^{-1}(\boldsymbol{\xi}, \dot{\boldsymbol{\xi}})[\mathbf{u}_\xi - \mathbf{B}(\boldsymbol{\xi}, \dot{\boldsymbol{\xi}})] - \hat{\mathbf{F}}_u \tag{11}$$

The inputs to the drone can be specified by the desired thrust force magnitude T_D^d and the desired Euler Angles $\boldsymbol{\Theta}^d$. These desired values can be determined by the kinematic transformation presented in our previous work [8],

$$T_D^d = ||\mathbf{u}_d||, \;\; \boldsymbol{\Theta}^d = f(\boldsymbol{\xi}, \mathbf{u}_d) \tag{12}$$

with $||.||$ denotes the norm of a vector and $f : \mathbb{R}^3 \times \mathbb{R}^3 \rightarrow \mathbb{R}^3$ is a nonlinear function. These desired values are the inputs for the drone's inner loops that are assumed to be stable and high performing control loops.

D. Stability Analysis

Replacing the control law $\mathbf{u}_d$, designed as (11), in the system nonlinear dynamics (3), the closed loop dynamics can be read as:

$$\ddot{\xi} = \mathbf{u}_\xi + \mathbf{A}(\boldsymbol{\xi}, \dot{\boldsymbol{\xi}}) * \Delta \mathbf{F}_u \tag{13}$$

where $\Delta \mathbf{F}_u = \mathbf{F}_u - \hat{\mathbf{F}}_u$ is the estimation error vector of the unknown forces. It could as well, be considered as source of disturbance and uncertainty.
Considering the following representation,

$$\mathbf{d}_u = \mathbf{A}(\boldsymbol{\xi}, \dot{\boldsymbol{\xi}}) * \Delta \mathbf{F}_u \tag{14}$$

is assumed to be bounded model uncertainty vector. This assumption may be achieved if the flying operation is constrained in the region $\boldsymbol{\Omega}$. This was validated by multiple simulations and we were able to obtain upper bounds of the uncertainties in (14).
The stability analysis is carried out using lyapunov stability theory for each loop $q \in \{r, \eta, \beta\}$. We define the Lyapunov function candidate as:

$$V_q = \frac{1}{2} S_q S_q \tag{15}$$

Its time derivative is calculated as:

$$\begin{aligned} \dot{V}_q &= S_q(\ddot{e}_q + \alpha_{1,q}\dot{e}_q + \alpha_{0,q}e) \\ &= S_q(-k_q sgn(S_q) + d_{u,q}) \\ &\leq -(k_q - |d_{u,q}|)|S_q| \end{aligned} \tag{16}$$

The gain k_q must be chosen so that $k_q \geq |d_{u,q}|$ for each $q \in \{r, \eta, \beta\}$. Using Lyapunov's direct method, it can be concluded that the equilibrium at the origin $S_q = 0$ is globally asymptotically stable because V_q is clearly positive-definite and $\dot{V}_q$ is negative-definite. Therefore, S_q tends to zero as time tends to infinity, and all trajectories starting off the sliding surface $S_q = 0$ must reach it in finite time and then remain on this surface. When sliding mode occurs on the sliding surface (6), $S_q = \dot{S}_q = 0$, and as a result, the dynamic behavior of the tracking problem can be equivalently governed by;

$$\dot{S}_q = 0 \Rightarrow \ddot{e}_q = -\alpha_{1,q}\dot{e}_q - \alpha_{0,q}e_q \tag{17}$$

It could be seen easily that if the parameters $\alpha_{1,q}$ and $\alpha_{0,q}$ are chosen such that:

$$P_q(s) = s^2 + \alpha_{1,q}s + \alpha_{0,q} \tag{18}$$

is Hulwitz polynomial, the tracking error e_q is stable and converges exponentially to zero.
Finally, the chattering phenomena of SMC is undesirable in practice, to eliminate and mitigate it we have replaced the discontinuous function sgn in (7) by smooth continuous hyperbolic tangent function $tanh$, Thus the intermediate control input $u_{\xi,q}$ for each $q \in \{r, \eta, \beta\}$ becomes as follows:

$$u_{\xi,q} = \ddot{q}_d - \alpha_{1,q}\dot{e_q} - \alpha_{0,q}e_q - \boldsymbol{k}_q \mathbf{tanh}(\frac{\boldsymbol{S}_q}{\gamma_q}) \tag{19}$$

with γ_q is a tuning parameter that takes values inside the interval (0, 1] and it allows one to satisfy a trade-off between control effectiveness and chattering attenuation.

E. SMC Tuning

The tuning parameters of the sliding surface in (6) are chosen using pole placement methodology, so the polynomial $P_q(s)$ in (18) is Hulwitz for each loop $q \in \{r, \eta, \beta\}$:

$$\alpha_{1,q} = 1.4w_q, \alpha_{0,q} = w_q^2$$

In this way, the closed loops achieve a second order time response with overshoot less than 5%. The natural frequencies are tuned such that $w_r = 10rd/s$ is higher than $w_\eta = 4rd/s$ and $w_\beta = 5rd/s$. This is because the reel-in and reel-out of the tether is controlled by the on-ground station motor-winch. This actuator is very fast and accurate compared to the drone that acts on the η-loop and β-loop.

IV. Simulation Environment

Using a realistic simulator that we have developed, the performance of the proposed control strategy is evaluated. Fig. 3 illustrates the different blocks of this simulator:

- **Drone Block-** In addition to the six degrees of freedom dynamics, this model also accounts for communication delays, inner control loops, battery model, aerodynamic forces due to the drone's body, and the four actuators' motors and propellers model. We implement the ROS/PX4 architecture which is used in our Lab for simulation purposes. More details are described in our article [8].
  To further study the robustness, we have included realistic modeling errors. Specifically, we have considered variations in battery voltage that result in an error between the desired thrust force T_D^d and the simulated generated force T_D^s, represented by $T_D^d - T_D^s$. This error is depicted in Fig. 8 and is associated with the uncertainties in $\mathbf{F}_p$.
- **On-ground Winch-** The on-ground station motor-winch subsystem is approximated as a fast first order dynamics:

  $$\dot{u}_{s,r} = \frac{1}{\tau_{u_r}}(u_{d,r} - u_{s,r}) \tag{20}$$

  with $u_{s,r}$ being the simulated on-ground motor torque. In simulation testing, $F_f = 0.4sgn(\dot{r})$ is represented by a classical static friction model.
- **Magnus Wing-** Simulations are conducted using this block to investigate the robustness of the control strategy against turbulent wind. The aerodynamic forces modeled as in [11] reads:

  $$\mathbf{F}_a := \mathbf{F}_a(\mathbf{v}_a, w_M, S_M) \tag{21}$$

where:

- w_M is the rotational speed of the Magnus motors,
- $S_M = 2l_M R_M$ is the projected surface area of the Magnus cylinder,
- $\mathbf{v}_a = \mathbf{v}_w - \mathbf{v}_k$ is the apparent wind velocity vector.

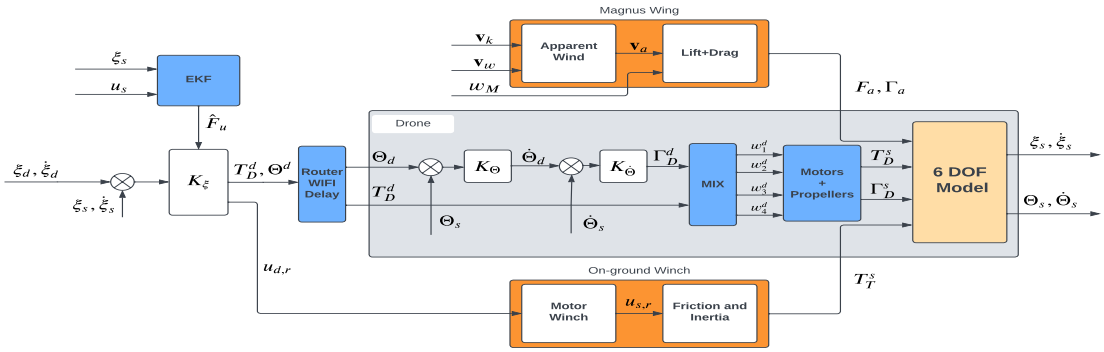

Fig. 3: Block diagram illustrating the simulation environment.

The proposed scenario considers a turbulent wind with speed vector $\mathbf{v}_w = [v_{w,x}, v_{w,y}, 0]^T$, displayed in Fig. 4. At the beginning, the wind is assumed to be directed in $x-$direction. After 6 sec a change in the wind direction is introduced.

The derivation of the time evolution of the wind speed model $v_{w,x}$ is developed in [12]. In the latest article, a wind speed model based on mixtures of Markov chain and stochastic differential equation has been proposed. The goal of the model is to produce hourly averaged wind speed sequences with statistical characteristics that are comparable to the wind speed that has been recorded.

In this present study, we investigate our control approach using a wind speed of class 2 wind turbulence and with an hourly average that falls between $(8, 9.4]$ m/s.

V. Results and Discussions

In this section, we present some simulation results to validate the performance of the (FF-SMC) control proposed in section II in comparison with the (FL-PID) control in [8]. The Integral Absolute Error (IAE) is used as a metric of comparison.

These control strategies can handle both the take-off and landing of the drone-based AWE system. The considered take-off/landing scenario is described in Table II, starting from an initial condition $\boldsymbol{\xi}_i = [0.5m, 0°, 20°]^T$.

Fig. 5 presents the estimated $\hat{\mathbf{F}}_u$ together with the assumed simulated values (assumed to be actual values) $\mathbf{F}_u$ generated by the realistic simulator models. The high level of aerodynamic disturbances depicted in the figure is noteworthy, especially considering the small prototype size. By comparing the curves in this figure, it can be seen that the applied EFK provides good estimation results in terms of accuracy and rapidity of convergence.

TABLE II: Desired trajectory $\boldsymbol{\xi}_d$,$\dot{\boldsymbol{\xi}}_d$

Time [s]	Operation Phase	$\dot{r}_d$[m/s]	$\dot{\eta}_d$[deg/s]	$\dot{\beta}_d$[deg/s]
$0 < t < 10$	Take-off	0.07	2	2.5
$10 \leq t < 25$	Hovering	0	0	0
$25 \leq t < 35$	Landing	-0.07	-2	-2.5
$35 \leq t < 40$	End of scenario	0	0	0

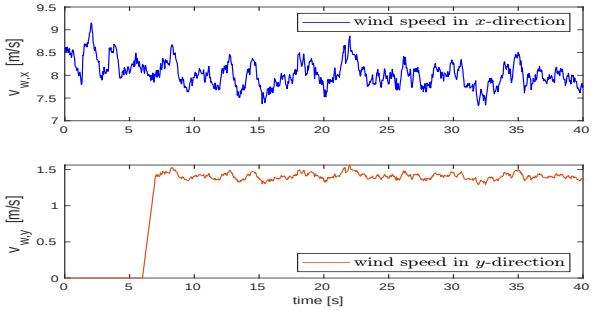

Fig. 4: Time evolution of the wind speed.

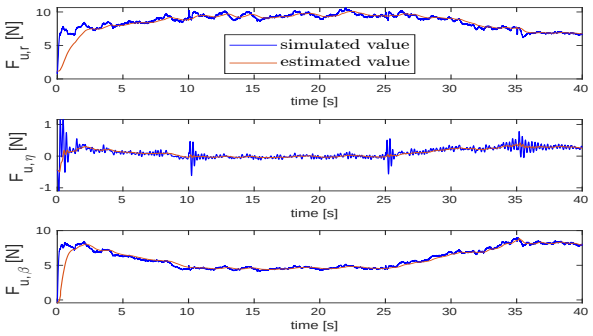

Fig. 5: Simulated and Estimated disturbance forces.

The sliding surface values for each loop over time in (6) are shown in Fig.6. The sliding surface values record non zero values during the beginning of the take-off phase, indicating a tracking error between the desired trajectory and the actual motion of the system. This is because of the significant disturbances during the begining of the operation which could be visualized by the big estimation error $\Delta\mathbf{F}_u$ at the starting period in Fig.5. However, as the system adapts and the control inputs are adjusted, the sliding surface value gradually decreases and reaches a stable value around zero, indicating successful tracking of the desired trajectory.

Table III shows the IAE values of each control strategy. The lower values of IAE when controlling the system by (FF-SMC) compared to that when implementing the (FF-PID) emphasize that (FF-SMC) reaches better accuracy than (FL-PID), especially in r and β dimensions.

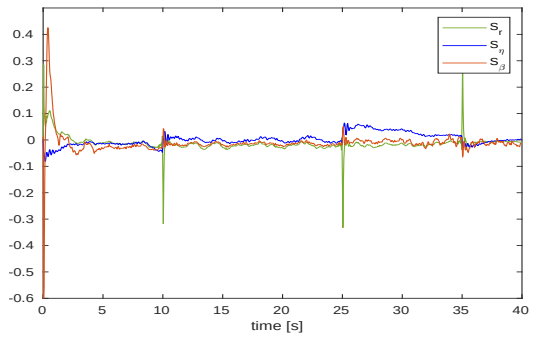

Fig. 6: Sliding surface trajectory

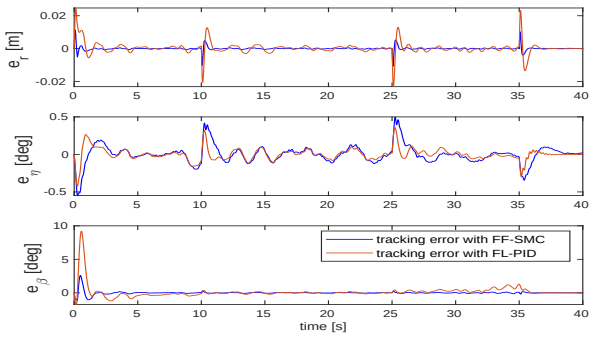

Fig. 7: Trajectory tracking errors of (FF-SMC) and (FL-PID).

TABLE III: IAE metric values

IAE	r	η	β
(FF-SMC)	8.03	26.73	25.62
(FL-PID	35.76	18.20	120.96

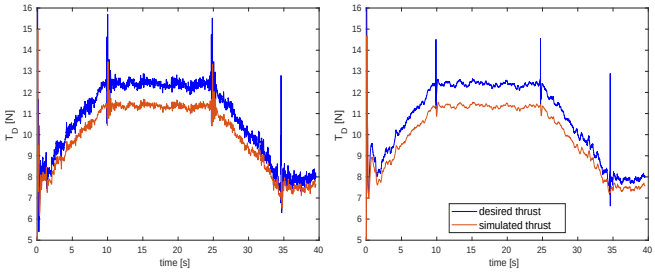

(a) (b)

Fig. 8: Drone's simulated and desired thrust. (a) system controlled by (FF-SMC), (b) System controlled by (FL-PID).

Moreover, to show clearly the performance and robustness of the (FF-SMC) control strategy compared to that of (FL-PID) control strategy, the time evolution of the tracking errors $\boldsymbol{\xi}_s - \boldsymbol{\xi}_d$ are plotted in Fig. 7. This figure shows that the system controlled by (FF-SMC) is more stable and robust in the transient state (fewer oscillations and less overshoots) against wind turbulence. The choice to control the system using a sliding mode approach is justified by its ability to improve robustness. Additionally, despite the estimated unknown forces not being exactly the same as the actual forces (as shown in Fig. 5), incorporating this estimation into the control strategy improves steady-state tracking performance.

It is evident that the (FF-SMC) control law allows for good tracking despite model uncertainties and disturbances, but at the cost of increased control activity, as demonstrated by the time evolution of the drone's thrust in Fig. 8.

VI. Conclusion and Perspective

In this research, a robust nonlinear controller was proposed for the 3D trajectory following process applied to drone-based airborne wind energy systems. The proposed controller was based on the combination of the sliding mode control and feed-forward technique. The suggested controller was compared to our previously proposed feedback linearization control law. We presented simulation results gathered using realistic simulator in order to evaluate our trajectory following control. Simulations are performed in presence of turbulent wind, modelling errors and unmodeled dynamics. The results confirm the expected performance and robustness increase of the designed control strategy against the systematic uncertainties and external disturbances compared to the feedback linearization technique.

In future works, we plan to apply high-order sliding mode controllers, such as the super twisting algorithm, to mitigate the chattering phenomenon. In addition, a more detailed robustness and stability analysis will be conducted. Moreover, optimization-based control allocation techniques are being studied in order to integrate the Magnus effect as an actuator, instead of only considering it as a source of disturbances, as is the case in this work.

References

[1] L. Fagiano, M. Quack, F. Bauer, L. Carnel, and E. Oland. Autonomous airborne wind energy systems: accomplishments and challenges. *Annual Review of Control, Robotics, and Autonomous Systems*, 2021.

[2] C. L. Archer and K. Caldeira. Global assessment of high-altitude wind power. *Energies*, page 307–319, 2009.

[3] R. Schmehl. *Airborne wind energy: advances in technology development and research*. Springer, 2018.

[4] C. Vermillion, M. Cobb, F. Lorenzo, R. Leuthold, M. Diehl, R. S.Smith, T. A.Wood, S. Rapp, R. Schmehl, D. Olinger, and M. Demetriou. Electricity in the air: Insights from two decades of advanced control research and experimental flight testing of airborne wind energy systems. *Annual Review of Control*, 52, 2021.

[5] D. Todeschini, L. Fagiano, C. Micheli, and A. Cattano. Control of rigid wing pumping airborne wind energy system in all operational phases. *Control Engineering Practice*, 111, 2021.

[6] A. Schanen, J. Dumon, N. Meslem, A. Hably, A. Nègre, and A. Sarazin. Tethered drone-based airborne wind energy system launching and retrieving. *Journal of Guidance, Control, and Dynamics*, 44, 2021.

[7] L. Fagiano and S. Schnez. On the take-off of airborne wind energy systems based on rigid wings. *Renewable Energy*, 107, 2017.

[8] Z. Azaki, J. Dumon, N. Meslem, A. Hably, and P. Susbielle. Modelling and control of a tethered drone for an awe application. *International Conference on Control, Automation and Diagnosis (ICCAD)*, 2022.

[9] H. K.Khalil. *Nonlinear Systems*. 3rd Edition, Prentice Hall, Upper Saddle River, 2002.

[10] N. Meslem, J. Dumon, A. Hably, A. El Ayachi, and A. Schanen. Online estimation of unknown aerodynamic forces acting on awe systems. *Intelligent Systems with Applications*, 16, 2022.

[11] Y. Gupta, J. Dumon, and A. Hably. Modeling and control of a magnus effect-based airborne wind energy system in crosswind maneuvers. *20th IFAC World Congress*, 50(1):13878–13885, 2017.

[12] J. Ma, M. Fouladirad, and A. Grall. Flexible wind speed generation model: Markov chain with an embedded diffusion process. *Energy*, 164:316–328, 2018.